Experimental realization of direct characterization of quantum dynamics

Zhi-Wei Wang,* Yong-Sheng Zhang, Yun-Feng Huang,† Xi-Feng Ren, and Guang-Can Guo
Key Laboratory of Quantum Information, University of Science and Technology of China, CAS, Hefei 230026, People's Republic of China

(Received 16 January 2007; published 20 April 2007)

We experimentally implement direct characterization of quantum dynamics (DCQD) algorithm of a single qubit proposed in M. Mohseni and D. A. Lidar [Phys. Rev. Lett. **97**, 170501 (2006)], which does not require quantum state tomography. The number of experimental configurations is reduced by a factor of 2 compared with that of standard quantum process tomography, which can be increased four times with an ideal Bell state analyzer. We combine the DCQD algorithm with maximum-likelihood estimation to give the physical characterization of quantum dynamics. It can also be applied to obtaining partial information about quantum dynamics.

DOI: 10.1103/PhysRevA.75.044304 PACS number(s): 03.67.Mn, 03.65.Wj, 42.50.Dv, 42.65.Lm

With the development of quantum information science [1], the characterization of the new quantum devices and quantum dynamics will play a more and more important role. One usual method is standard quantum process tomography (SQPT) [1–5], which involves preparing an ensemble of a number of a set of quantum states, subjecting each of them to the concerned quantum dynamics, and performing quantum state tomography [6–8] on the output states. An alternative to SQPT, ancilla-assisted process tomography (AAPT) [9,10], utilizing an extra ancilla system, involves preparation and quantum state tomography of the whole system including both the main and ancilla system.

However, two main issues are usually associated with the two methods mentioned above: first, the number of ensemble measurements grows exponentially with the degrees of freedom of the system; second, it is not able to acquire the information about the system directly. On the contrary, The information is often indirectly estimated via quantum state tomography.

To resolve the issues, Mohseni and Lidar [11] developed an algorithm for direct characterization of quantum dynamics (DCQD), which does not need quantum state tomography. It is required that the primary system be initially entangled with an ancilla system, and be subjected to the concerned quantum dynamics. The information about the dynamics is acquired through a certain set of error-detecting measurements.

In this paper, for experimental reasons, we only consider characterizing one-qubit quantum dynamics. The information about the quantum dynamics, represented with ε, can be completely obtained by inputing four two-qubit entangled states into the dynamics and performing certain Bell states measurements (BSMs) at the outputs. The process is illustrated in Fig. 1. The number of required experimental configurations is 16 for both SQPT and separable AAPT, and 4 for DCQD, while for quantum dynamics of multiqubit systems, the quadratic advantage of DCQD over SQPT and separable AAPT is more obvious [11–14].

The full characterization of a quantum dynamical map ε can be expressed as [1]

$$\varepsilon(\rho) = \sum_{m,n=0}^{3} \chi_{mn} E_m \rho E_n^{\dagger}. \tag{1}$$

Here $\{E_m\}_{m=0}^{3}$ are selected as the error operator basis identity operator and Pauli operators: $\{I,X,Y,Z\}$. $\{\chi_{mn}\}$ contains all information about the quantum dynamics. Our aim is to determine the matrix χ directly via experiment.

In the following, we will briefly introduce and modify the method presented in Ref. [11] to implement the process of acquiring the matrix χ (see Table I) conveniently in experiment. To determine the diagonal terms of the the matrix χ, referred to as *quantum dynamical population* in Ref. [11], let us prepare the maximally entangled state

$$|\phi^+\rangle = (|0_A 0_B\rangle + |1_A 1_B\rangle)/\sqrt{2}, \tag{2}$$

subject qubit A to the map ε, and perform the measurements of the observables $Z_A Z_B$ and $X_A X_B$ (equivalent to BSM). Since different output states corresponding to different possible errors of the quantum dynamics are mapped to different orthogonal subspaces of the total Hilbert space, the probabilities of obtaining the error-free outcome I, bit flip error X_A, phase flip error Z_A, and both phase and bit flip errors Y_A become

$$p_m = \mathrm{Tr}[P_{mZ}\varepsilon(\rho)] = \chi_{mm} (m = 0,1,2,3), \tag{3}$$

where

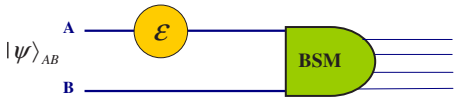

FIG. 1. (Color online) The sketch map of direct characterization of one-qubit quantum dynamics, involving inputing entangled state ψ_{AB}, the quantum map ε, and Bell state measurements (BSMs).

*Electronic address: sdzzwzw@mail.ustc.edu.cn
†Electronic address: hyf@ustc.edu.cn

TABLE I. The standard process for direct characterization of quantum dynamics for a single qubit (for the original table please see Ref. [11]), where $|\alpha| \neq |\beta| \neq 0$ and $\{|0\rangle,|1\rangle\}$, $\{|\pm\rangle\}$, $\{|\pm i\rangle\}$ are eigenstates of the Pauli operator Z, X, and Y.

Input state	Measurement	Output
$(\|0\rangle\|0\rangle+\|1\rangle\|1\rangle)/\sqrt{2}$	Z_AZ_B, X_AX_B	χ_{00}, χ_{11}, χ_{22}, χ_{33}
$\alpha\|0\rangle\|0\rangle+\beta\|1\rangle\|1\rangle$	Z_AZ_B, X_AX_B	χ_{03}, χ_{12}
$\alpha\|+\rangle\|0\rangle+\beta\|-\rangle\|1\rangle$	X_AZ_B, Z_AX_B	χ_{01}, χ_{23}
$\alpha\|+i\rangle\|0\rangle+\beta\|-i\rangle\|1\rangle$	Y_AZ_B, Z_AY_B	χ_{02}, χ_{13}

$$P_{0Z} = |\phi^+\rangle\langle\phi^+|, \quad P_{1Z} = |\psi^+\rangle\langle\psi^+|,$$

$$P_{2Z} = |\psi^-\rangle\langle\psi^-|, \quad P_{3Z} = |\phi^-\rangle\langle\phi^-| \tag{4}$$

are the four Bell states projection operators and $|\phi^\pm\rangle = (|0_A0_B\rangle \pm |1_A1_B\rangle)/\sqrt{2}$, $|\psi^\pm\rangle = (|0_A1_B\rangle \pm |1_A0_B\rangle)/\sqrt{2}$.

To acquire the off-diagonal elements of χ, which characterize the *coherence* in the quantum dynamical process, a set of BSMs are performed in order that only partial information about the system is obtained. For example, to determine χ_{03} and χ_{12}, the input state is

$$|\psi_Z\rangle = \alpha|0_A0_B\rangle + \beta|1_A1_B\rangle \tag{5}$$

with $|\alpha| \neq |\beta| \neq 0$. Bell state projection measurements are performed, which are represented with P_{mZ} $(m=0,1,2,3)$ in Eq. (4). Since we are not able to tell the difference between I and Z_A, X_A, and Y_A, the coherence between them is preserved. The result of BSM is

$$\begin{aligned}
\mathrm{Tr}[P_{0Z}\varepsilon(\rho)] &= 0.5[\chi_{00}M + \chi_{33}N + \Re(\chi_{03})U + \Im(\chi_{03})V], \\
\mathrm{Tr}[P_{3Z}\varepsilon(\rho)] &= 0.5[\chi_{00}N + \chi_{33}M + \Re(\chi_{03})U - \Im(\chi_{03})V], \\
\mathrm{Tr}[P_{1Z}\varepsilon(\rho)] &= 0.5[\chi_{11}M + \chi_{22}N - \Re(\chi_{12})V + \Im(\chi_{12})U], \\
\mathrm{Tr}[P_{2Z}\varepsilon(\rho)] &= 0.5[\chi_{11}N + \chi_{22}M + \Re(\chi_{12})V + \Im(\chi_{12})U],
\end{aligned} \tag{6}$$

where $U=2(|\alpha|^2-|\beta|^2)$, $V=4\,\mathrm{Im}(\alpha\beta^*)$, $M=|\alpha+\beta|^2$, and $N=|\alpha-\beta|^2$ can be obtained from the input state $|\psi_Z\rangle$.

In order to obtain the remaining coherent elements of χ, the basis of input states and measurements are properly changed (see Table I). For characterizing χ_{01} and χ_{23}, the input state is transformed into

$$|\psi_X\rangle = \alpha|+_A0_B\rangle + \beta|-_A1_B\rangle \tag{7}$$

with $|\pm\rangle = (|0\rangle \pm |1\rangle)/\sqrt{2}$ and BSM is transformed as the measurements of observables X_AZ_B and Z_AX_B. The results have the similar form to Eq. (6).

To determine χ_{02} and χ_{13}, we prepare the state

$$|\psi_Y\rangle = \alpha|+_iA0_B\rangle + \beta|-_iA1_B\rangle \tag{8}$$

with $|\pm i\rangle = (|0\rangle \pm i|1\rangle)/\sqrt{2}$ and measure BSM operators Y_AZ_B and Z_AY_B. Therefore the matrix χ containing the full information about the quantum dynamics can be directly obtained with four BSMs.

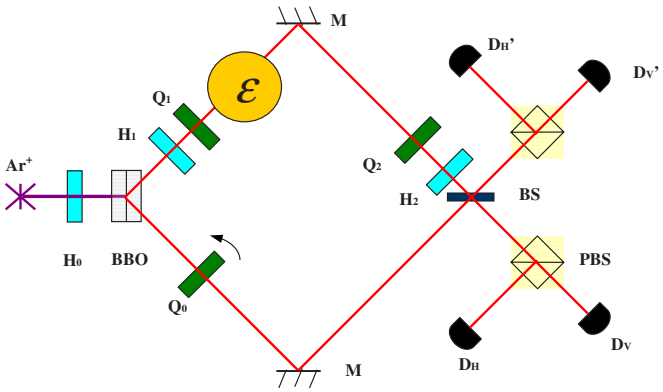

FIG. 2. (Color online) The experimental setup to implement direct characterization of quantum dynamics. The light produced by an Ar^+ laser is incident on BBO crystal. The entangled state Eq. (9) is produced via spontaneous parametric down-conversion, which can be adjusted with half wave plate (HWP) H_0 and quarter wave plate (QWP) Q_0. HWP H_1 and QWP Q_1 are used to prepare the required input states. The Hong-Ou-Mandel interferometer is used to perform the BSM. H_2 and Q_2 change the measurement basis from $\{|\psi^+\rangle, |\psi^-\rangle\}$ to $\{|\phi^+\rangle, |\phi^-\rangle\}$. To detect the photon pairs, we use interference filter (bandwidth 4.62 nm), single-photon detectors, and two-photon coincidence.

Experimentally, we use linear optics to implement the DCQD algorithm. The experiment setup is shown in Fig. 2. A 0.59-mm-thick β-barium borate (BBO) crystal arranged in the Kwiat-type configuration [6] is pumped by a 351.1-nm laser beam produced by an Ar^+ laser. Through the spontaneous parametric down-conversion (SPDC) process, a nonmaximally entangled state

$$|\psi_0\rangle = a|HH\rangle + e^{i\phi}b|VV\rangle \tag{9}$$

is produced, where the normalized real numbers a and b can be determined by the half wave plate (HWP) H_0 in the pump beam and the phase $e^{i\phi}$ can be adjusted with the tiltable quarter wave plate (QWP) Q_0. $|H\rangle$ and $|V\rangle$ represent horizontal and vertical polarization of the photons, corresponding to $|0\rangle$ and $|1\rangle$ in the theoretical introduction. We use the Hong-Ou-Mandel interferometer [15] to perform the BSM [16]. HWP H_1 and QWP Q_1 are used to prepare the input states in Table I. The coincidence of D_H and D_V (D'_H and D'_V) denotes the measurement of $|\psi^+\rangle$ and that of D_H and D'_V (D_H and D'_V) represents measuring the state $|\psi^-\rangle$ [17]. Since we can only discriminate two of the four Bell states simultaneously, we have to change the basis of BSM with the aid of H_2 and Q_2 to perform the remaining Bell states measurements. The steps are similar to the above for the transformed BSM.

In the experiment, we investigate several quantum dynamical processes, including both trace-preserving map, identity, a unitary rotation operator, and non-trace-preserving map, a partial polarizer. First, we use the steps introduced above to perform DCQD measurements for these processes. Usually, DCQD will lead to an unphysical process matrix. For physicality, it is necessary that the map be completely positive and not increase the trace. We use the maximum-likelihood estimation by finding a positive and Hermitian

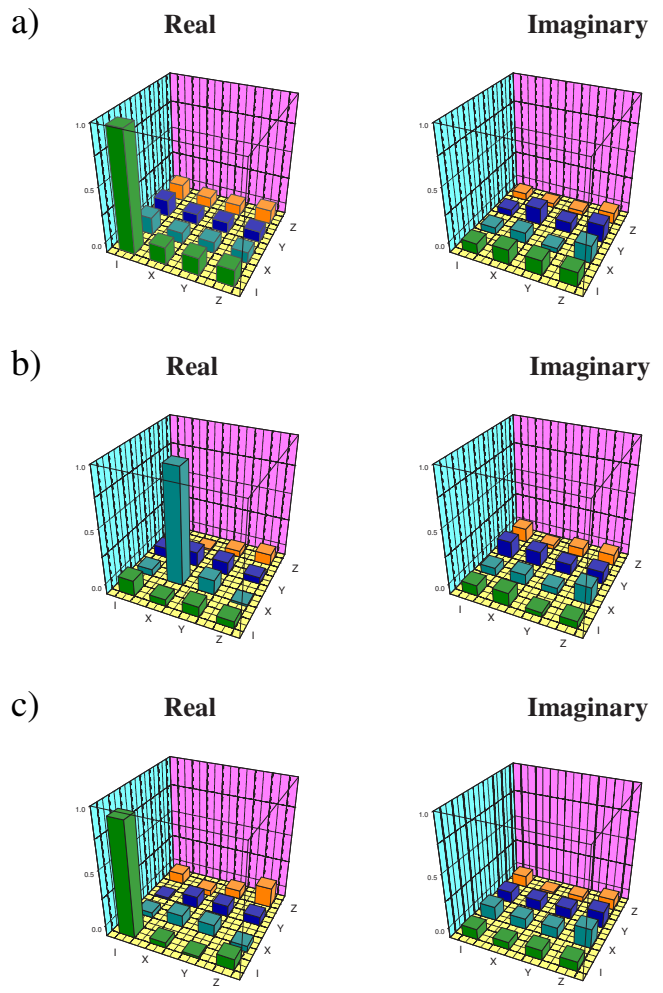

FIG. 3. (Color online) χ matrices obtained from direct characterization of quantum dynamics (DCQD) for (a) identity, (b) unitary, and (c) partial polarizer process.

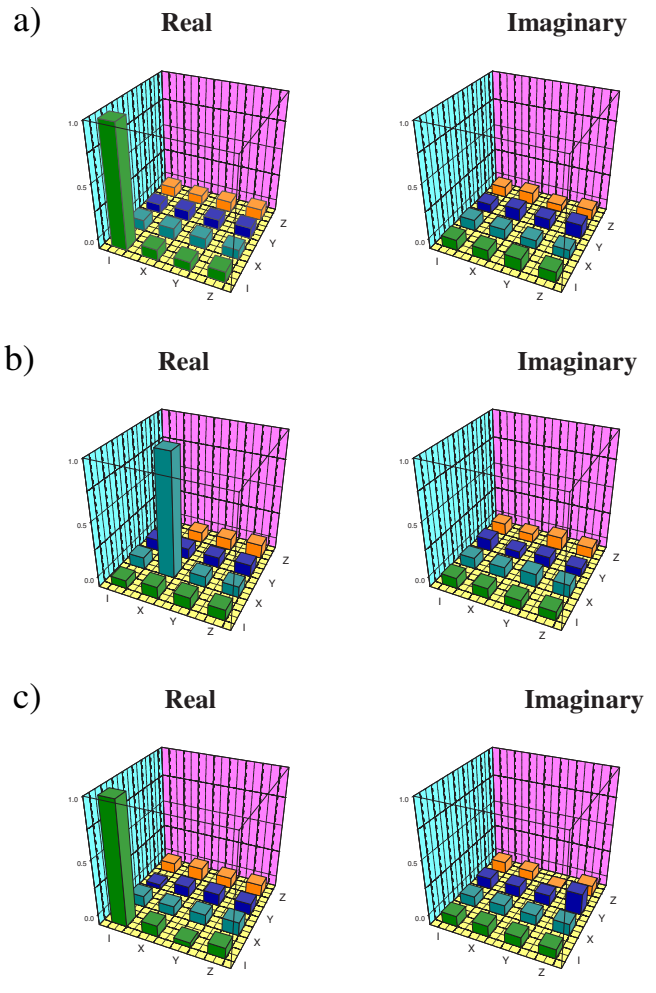

FIG. 4. (Color online) χ matrices obtained from standard quantum process tomography (SQPT) for (a) identity, (b) unitary, and (c) partial polarizer process.

matrix which is the closest fit in a least-squares sense to convert the experimental data into physical process matrices [7,19]. The real and imaginary part of matrix χ are shown in Fig. 3.

Next, for the same processes, we also perform SQPT measurements [18]: we prepare a set of states $\{|H\rangle,|V\rangle,|D\rangle,|R\rangle\}$ for the polarization qubit, where $|D\rangle$ and $|R\rangle$ correspond to $|+\rangle$ and $|+i\rangle$; each of them is subject to the process ε and quantum state tomography is performed to determine the output states; at last, we obtain the matrix χ using the calculating method introduced in Ref. [1] and maximum-likelihood estimation [7,19]. The results are shown in Fig. 4.

Finally, by the comparison of the data in Fig. 3 and 4, we can see that the results of DCQD and those of SQPT are in good agreement. The average process fidelity F_p [10] between these two methods are $98.8\pm0.6\%$ for the identity map. For the unitary map, we select a HWP with the angle between its axis and the vertical axis 45°. The process fidelity is $97.9\pm0.6\%$. For the partial polarizer, we insert two pieces of tilted microscope slides into the place of ε in Fig. 2. The process fidelity is $96.6\pm0.7\%$ [the χ matrices of partial polarizer in Figs. 3(c) and 4(c) are normalized].

For every measurement, the interference visibilities of the Hong-Ou-Mandel interferometer are more than 97%. Hence the nonperfect interference is the main cause of the decrease in the process fidelity. Therefore based on the comparison between SQPT and DCQD, DCQD is demonstrated experimentally to be one effective way of characterizing the quantum dynamics up to the current experimental accuracy.

Due to the restriction of our experimental setup, we cannot perform complete Bell state discrimination simultaneously, so our experiment is not able to realize the quadratic advantage over SQPT. However, the number of experimental configurations is still reduced by a factor of 2 compared with that of SQPT for characterizing one-qubit quantum dynamics. Using the other method [20–22] to perform complete BSM, this advantage will be revealed.

DCQD can also be used to extract partial information about the quantum dynamics with fewer measurements when we do not need the full characterization of quantum dynamics or we have *a priori*knowledge about the system. For example, we can obtain the *quantum dynamical population* χ_{mm} or the coherent elements χ_{mn} in one BSM. Generalization to other quantum systems, we can determine some important physical quantities associated with the elements of χ, such as the longitudinal relaxation time and the transverse relaxation

time in one BSM [11]. DCQD has important application in characterization of the dynamics of quantum, which has unknown interaction with its environment. Such characterization of dynamics would be essential for many fields in quantum information science. It can also be applied to generalized quantum dense coding and Hamiltonian identification tasks [13,23].

In summary, we experimentally implement the DCQD algorithm for one-qubit quantum dynamics using linear optics without quantum state tomography. By the comparison between the results of DCQD and those of SQPT, it is demonstrated that DCQD is an effective way of directly characterizing quantum dynamics and is able to reduce the number of experimental configurations by a factor of 2. The main errors come from the nonperfect interference and the errors introduced by the optical components. DCQD can also be used to extract partial information about the dynamics without the full characterization of it. It would be essential for many fields in quantum information science.

This work was funded by the National Fundamental Research Program, National Natural Science Foundation of China (Grants No. 60121503, No. 10674127), Innovation Funds from Chinese Academy of Sciences, and Program for New Century Excellent Talents in University.

[1] M. A Nielsen and I. L. Chuang, *Quantum Computation and Quantum Information* (Cambridge University Press, Cambridge, UK, 2001).
[2] J. F. Poyatos, J. I. Cirac, and P. Zoller, Phys. Rev. Lett. **78**, 390 (1997).
[3] I. L. Chuang and M. A Nielsen, J. Mod. Opt. **44**, 2455 (1997).
[4] A. M. Childs, I. L. Chuang, and D. W. Leung, Phys. Rev. A **64**, 012314 (2001).
[5] M. W. Mitchell C. W. Ellenor, S. Schneider, and A. M. Steinberg, Phys. Rev. Lett. **91**, 120402 (2003).
[6] A. G. White, D. F. V James, P. H. Eberhard, and P. G. Kwiat, Phys. Rev. Lett. **83**, 3103 (1999).
[7] D. F. V James, P. G. Kwiat, W. J. Munro, and A. G. White, Phys. Rev. A **64**, 052312 (2001).
[8] R. T. Thew, K. Nemoto, and A. G. White, W. J. Munro, Phys. Rev. A **66**, 012303 (2002).
[9] G. M. D'Ariano and P. LoPresti, Phys. Rev. Lett. **86**, 4195 (2001).
[10] J. B. Altepeter *et al.*, Phys. Rev. Lett. **90**, 193601 (2003).
[11] M. Mohseni and D. A. Lidar, Phys. Rev. Lett. **97**, 170501 (2006).
[12] M. Mohseni and D. A. Lidar, e-print quant-ph/0601033.
[13] M. Mohseni and D. A. Lidar, e-print quant-ph/0601034.
[14] M. Ziman, e-print quant-ph/0603151; M. Mohseni and D. A. Lidar, e-print quant-ph/0604114.
[15] C. K. Hong, Z. Y. Ou, and L. Mandel, Phys. Rev. Lett. **59**, 2044 (1987).
[16] M. Michler, K. Mattle, H. Weinfurter, and A. Zeilinger, Phys. Rev. A **53**, R1209 (1996).
[17] K. Mattle, H. Weinfurter, P. G. Kwiat, and A. Zeilinger, Phys. Rev. Lett. **76**, 4656 (1996).
[18] Since the number of experimental configurations of SQPT is the same as that of separable AAPT, we only perform SQPT for the quantum dynamical process in the experiment.
[19] J. L. O'Brien, G. J. Pryde, A. Gilchrist, D. F. V. James, N. K. Langford, T. C. Ralph, and A. G. White, Phys. Rev. Lett. **93**, 080502 (2004).
[20] P. G. Kwiat and H. Weinfurter, Phys. Rev. A **58**, R2623 (1998).
[21] C. Schuck, G. Huber, C. Kurtsiefer, and H. Weinfurter, Phys. Rev. Lett. **96**, 190501 (2006).
[22] M. Barbieri, G. Vallone, P. Mataloni, and F. De Martini, e-print quant-ph/0609080.
[23] M. Mohseni, A. T. Rezakhani, and D. A. Lidar (unpublished).